CHEMICAL PHYSICS

Chemical trigger toward phase separation in the aqueous Al(III) system revealed

Miodrag J. Lukić[1], Eduard Wiedenbeck[2], Holger Reiner[2], Denis Gebauer[1]*

Although Al(III) hydrolysis, condensation, and nucleation play pivotal roles in the synthesis of Al-based compounds and determine their chemical behavior, we still lack experimental evidence regarding the chemistry of nucleation from solution. Here, by combining advanced titration assays, high-resolution transmission electron microscopy (HR-TEM), and ^{27}Al–nuclear magnetic resonance spectroscopy, we show that highly dynamic solute prenucleation clusters (PNCs) are fundamental precursors of nanosolid formation. Chemical changes from olation to oxolation bridging within PNCs rely on the formation of tetrahedral AlO_4 in solution and trigger phase separation at low driving force (supersaturation). This does not include the formation of Keggin-Al_{13} ions, at least during the earliest stages. The PNC pathway of the formation of Al(III) (oxy)(hydr)oxides offers new possibilities toward the development of strategies for controlling the entire crystallization process.

INTRODUCTION

The cascade of hydrolysis-(polymerization/condensation)-nucleation in the aqueous Al(III) system plays a central role during the formation of natural Al flocs (*1*), immobilization of heavy metal ions (*2*), Al-related health issues (*3*), development of efficient and nontoxic vaccine adjuvants (*4*), Al-based batteries (*5*), and the formation of versatile metal-organic frameworks (*6*, *7*). Although extensively studied, several important questions regarding the nucleation of distinct Al compounds from aqueous solutions are still under debate. The transformation from octahedral to tetrahedral coordination environments toward the formation of Keggin-Al_{13} species and the role of small oligomeric species during the early stages of Al(III) nucleation from solution remain unknown. Keggin-Al_{13} ions consist of a central tetra-coordinated AlO_4 unit with a shell of 12 octahedrally coordinated AlO_6 units that are organized in four trimers. Understanding the formation mechanism of Keggin-Al_{13} species is a topical issue, since these species are involved in many natural processes and engineering applications (*1*, *2*). Previous experimental and theoretical findings suggested a progressive reduction in coordination number due to the proximity of the deprotonation constants of the Al(III) hydroxo complexes (*8*). Along with that, the penta-coordinated $[Al(H_2O)_4OH_{(aq)}]^{2+}$complex serves as a plausible intermediate toward the formation of a tetrahedrally coordinated AlO_4 unit in the Keggin-Al_{13} structure (*9*). The role of oligomeric Al(III) species thereby directly relates to the mechanism of the formation of tetrahedral coordination environments. Aiming to reconcile the interpretations of different experimental results, these small polynuclear species were assumed to be a series of transient dynamic intermediates that transform into Keggin-Al_{13} ions (*10*), where aging processes, e.g., via direct addition of trimer and tetramer polycations (*11*) or high-temperature treatments and the addition of counter anions, are required (*10*). Nevertheless, several authors questioned the existence of small oligomeric species like dimers in solution based on potentiometric studies (*12*). However, their detection may have been hampered by low total Al(III) concentrations and inherent restrictions of the used method (*13*). Recent theoretical studies implied the existence of stable Al(III) clusters (*14*), and the importance of tetrahedral $[Al(H_2O)(OH)_3]^0$ species for the formation of Keggin-Al_{13} ions at moderate base titration rates was suggested on the basis of computer simulations (*15*).

Classical nucleation theory (CNT) successfully explains observations of $Al(OH)_3$ formation from caustic aluminate solutions; however, for instance, CNT cannot adequately explain the finding of different induction times in the presence of Na^+ and K^+ counter cations (*16*). By monitoring the density change of a drying droplet of different α-Keggin heteropoly acids, liquid-liquid phase separation was suggested as a first step in the crystallization process (*17*). "Nonclassical" nucleation via prenucleation clusters (PNCs) explains experimental observations of nucleation in the aqueous Fe(III) system, which is also a hydrolyzing/condensating metal cation, suggesting that the chemistry and the dynamics of species present at the different stages of precipitation determine the onset of liquid-liquid phase separation, rather than their size as in CNT (*18*, *19*). This implies that a similar behavior could be expected for the Al(III) system, although the chemistries of Fe(III) and Al(III) differ especially in terms of the initial hydrolysis constants (also see above). It should be noted that with respect to the PNC pathway, Keggin-Al_{13} ions should be considered phase-separated nanosolids occurring as later intermediates in the nucleation mechanism that undergo further aggregation processes due to their high structural stability and slow dynamics (*20*). Energetic calculations indicating that Keggin-Al_{13} species lie close in energy to the solid Al-(oxy)hydroxide phase corroborate this interpretation (*21*).

RESULTS

Potentiometric titrations at constant pH and high-resolution transmission electron microscopy

Potentiometric studies of Al(III) hydrolysis usually adopted methods where the pH is increased; however, here, we take advantage of a pH-constant titration assay, slowly increasing the concentration of Al(III) at low driving force for phase separation, inspired by the literature in (*19*). Figure 1A shows that the obtained titration curves in the pH range from 3.9 to 4.6. Below pH 3.9, the consumed amount of base linearly scales with the added $[Al^{3+}]$, bending upward

[1]Institute of Inorganic Chemistry, Leibniz University Hannover, Callinst. 9, 30167 Hannover, Germany. [2]University of Konstanz, Department of Chemistry, Physical Chemistry, Konstanz, Germany.
*Corresponding author. Email: gebauer@acc.uni-hannover.de

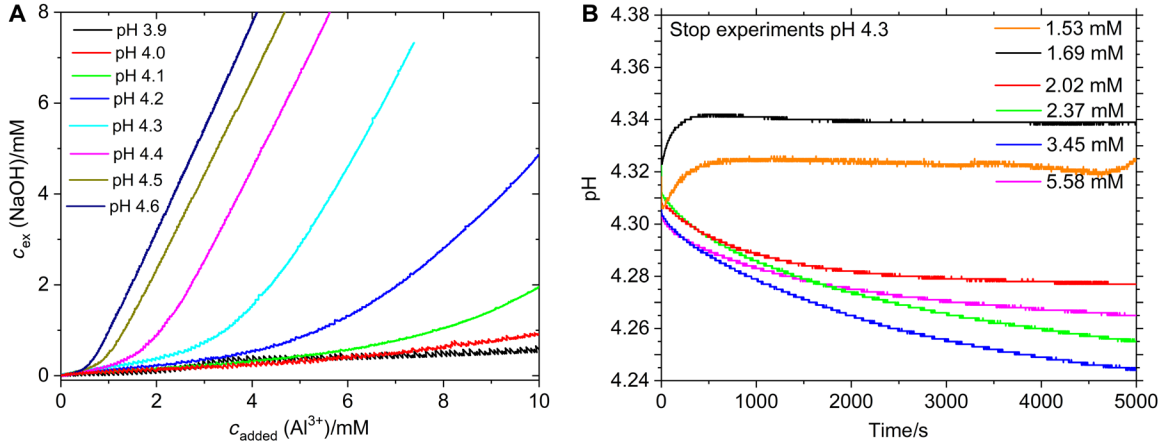

Fig. 1. Titration experiments for the assessment of distinct Al(III) hydrolysis regimes. (**A**) Titration curves at different pH values showing the amount of consumed base to keep the pH value constant upon Al(III) addition, corrected for the amount of the base required for adjusting the pH of the added solution. After the first linear part, there is an upward bending, indicating a transition between at least two hydrolysis regimes. (**B**) Stop experiments at pH 4.3 provide insight into this transition regime by showing the pH evolution after stopped Al(III) dosing and pH-constant titration. The monotonous decrease of pH at and above ~2 mM overlaps with the change in the hydrolysis regime and shows that the system is not in equilibrium anymore, defining the postnucleation regime.

at higher concentrations, pointing toward the existence of two hydrolysis regimes. The second regime shows a substantially increased amount of consumed base required to keep the pH constant due to the extensive H^+ release, which progressively shifts toward lower [Al^{3+}] with increasing pH. According to calculations of equilibrium constants from asymptotes of the initial linear regime (see fig. S1 and table S1), the pK_a (where K_a is the acid dissociation constant) value of 5.13 agrees well with literature values for the first deprotonation reaction of $[Al(H_2O)_6]^{3+}$ (*22*). There are no kinetic effects that might affect this thermodynamic analysis (see fig. S2). "Stop experiments" provide important insight into the transition regime toward the identified second hydrolysis regime, where the Al(III) addition and the automatic base titration for maintaining the constant pH are stopped at specific concentrations during titrations at pH 4.3, and the pH evolution profile is continuously monitored (Fig. 1B). This shows that up to 1.69 mM, there is no decrease in pH value after stopping the titrations, while at concentrations higher than ~2 mM, the pH value continuously decreases, albeit the Al(III) addition has been stopped, illustrating that the hydrolysis reaction proceeded independently of further Al(III) addition. This implies that below ~2 mM, the system is in a state of (meta)stable prenucleation equilibrium (*20*). Above that concentration, the system is not in equilibrium anymore, where the continuing pH change provides evidence of, e.g., ongoing condensation, aggregation, and olation to oxolation reactions, indicative of transformation/growth of aluminum species. Thus, the stop experiments establish the transition between the prenucleation (equilibrium) and postnucleation (nonequilibrium) stages. The corresponding limit overlaps with the transition between the hydrolysis regimes observed at pH 4.3 (see fig. S3).

High-resolution transmission electron microscopy (HR-TEM) inspection of a sample drawn in the prenucleation regime at pH 4.3 reveals the existence of a large population of uniform, single spherical species with sizes of several nanometers (Fig. 2, A and B), similar to already reported PNCs for different systems (*19*, *20*). However, the drying step during the sample preparation for TEM induces structural changes and even partial crystallization of these entities, which explains the appearance of lattice fringes in some of the nanoscopic

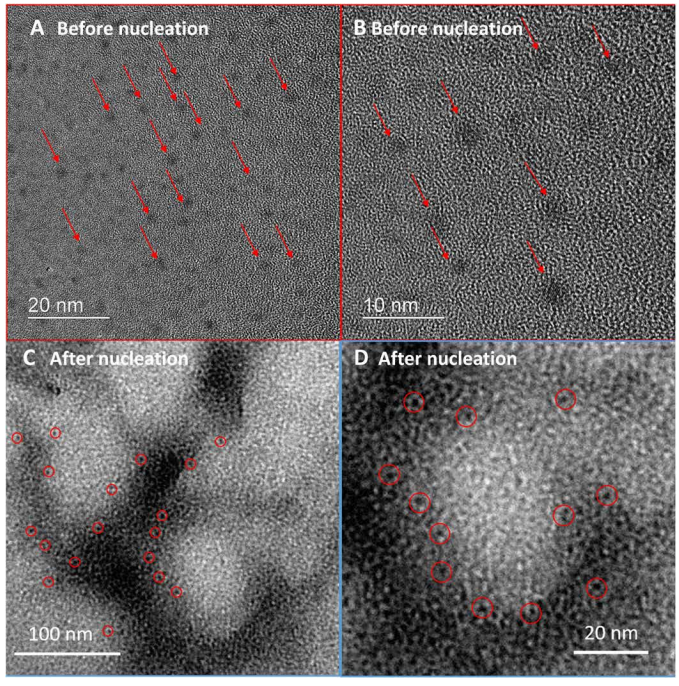

Fig. 2. TEM of prenucleation and postnucleation stages of Al(III) (oxy)hydroxide precipitation. (**A**) HR-TEM micrographs of samples drawn from the prenucleation regime at 1.69 mM [Al^{3+}] at pH 4.3 and (**B**) at higher magnification. The entities isolated from the prenucleation stages are well separated, with some drying artifacts sporadically present (see fig. S4); note that the drying step induces phase separation and transformations, leading to the occurrence of lattice fringes in some of the particles. (**C**) The sample drawn after nucleation at 4 mM shows aggregation of small phase-separated entities, the sizes of which relate to those isolated from the prenucleation regime, and (**D**) a magnified region better showing the constituting species (red circles highlight some of them).

features. At a later stage of Al(III) hydrolysis, namely, after the transition to the second hydrolysis regime (see above and Fig. 1), a network of randomly attached particles forms at ~4 mM [Al^{3+}], which clearly indicates aggregation of nanoscopic postnucleation entities (Fig. 2C).

This shows that the transition observed in pH-constant titration curves, which is inherently related to the onset of phase separation established in stop experiments (Fig. 1B), additionally leads to aggregative processes in the system. The ion activity product (IAP) of Al^{3+} and OH^- at the point of the transition between prenucleation and postnucleation regimes, i.e., when the system is not in a state of equilibrium of aluminum hydrolysis anymore (as determined in stop experiments at pH 4.3; see above), can be calculated from the titration data. The critical IAP for phase separation is $[Al^{3+}]\cdot[OH^-]^3 \approx 1.57\cdot10^{-32}\ M^2$. This value essentially agrees with the solubility product of aluminum hydroxide, $K_{sp} \approx 31.8$ (*23*), suggesting that we, indeed, identify the moment of phase separation.

^{27}Al–nuclear magnetic resonance spectroscopy

Liquid ^{27}Al–nuclear magnetic resonance (NMR) spectroscopy studies provide further insight into the Al(III) hydrolysis behavior underlying the above observations. First, we explored a constant total Al(III) concentration (~2.2 mM) at different pH values (4.0, 4.2, 4.4, and 4.6). In the prenucleation regime, i.e., at pH 4.0 and 4.2, only the resonance of monomeric species at 1 part per million (ppm) [with respect to 10 mM $Al(NO_3)_3{\cdot}9H_2O$ at pH 2 as an external standard (*24*); see figs. S5 and S6] appears. At pH 4.4 and 4.6, i.e., in the postnucleation regime, besides monomeric species, there is a resonance at ~63.7 ppm (Fig. 3), which corresponds to tetrahedrally coordinated AlO_4 (*13*). Upon pH increase from 4.0 to 4.6, the chemical shift and linewidth of the resonance due to the monomer also increases (fig. S7). Similar behavior and the consumption of monomeric Al(III) complexes were assigned to the formation of $[Al(OH)]^{2+}$, $[Al(OH)_2]^+$, or Al(III) dimers, although new resonances were not observed (*25*). However, despite further inconsistencies (*26*), Swaddle *et al.* (*9*) proposed that this would be due to the formation of the penta-coordinated $[Al(H_2O)_4(OH)]^{2+}$ complex, the signal of which might be lost in ^{27}Al-NMR because of rapid quadrupolar relaxation of the nucleus, causing extreme broadening of ^{27}Al resonances from low-symmetry sites. In view of the titration (Fig. 1) and TEM data (Fig. 2), we propose that the observed NMR behavior (Fig. 3) actually originates from the formation of highly dynamic Al(III) olation PNCs, where no separate oligomer resonance is found because of corresponding exchanges between olated (hydroxo-bridged) PNCs and monomeric species, causing a minor shift of the resonance due to monomers, which is indeed observed (fig. S7B). At higher pH, metal centers within olation PNCs may exhibit lower coordination numbers, i.e., pentahedral environments (see below) due to the cooperative character of Al(III) hydrolysis, which would also yield a minor shift and broadening of the octahedral resonance position. Our data, however, provide no unambiguous evidence of the existence of such penta-coordinated species.

The interpretation toward the role of the formation of distinct coordination environments during phase separation can be substantiated by exploring the transition region between the two hydrolysis regimes further by gradually changing the concentration of Al(III) at pH 4.2 and 4.4 (Fig. 4). At low concentrations, only the resonance at ~1 ppm (cf. Fig. 3A) appears, without any new signals in the spectral region of 3 to 5 ppm. The resonance originating from the tetrahedral AlO_4 environment clearly appears at ~5.6 mM $[Al^{3+}]$ at pH 4.2 (Fig. 4B) and at ~1.9 mM $[Al^{3+}]$ at pH 4.4 (fig. S8). These concentrations lie in the transition between the two hydrolysis regimes also observed in the titration curves (Fig. 4C) and can be assigned to the point of phase separation. This inherent correlation between chemical changes as evidenced by NMR, and the irreversible progress of the hydrolysis only in the postnucleation regime as evidenced by the titrations (Fig. 1), agrees with the notions of the PNC theory, that is, chemical changes that affect the dynamics of the species forming govern the onset of phase separation, rather than their sizes (*18*, *20*). The integral intensity of the AlO_4 resonance linearly increases with concentration (Fig. 4D) after nucleation, while that of octahedrally coordinated species changes the slope, i.e., deviates from the linear prenucleation increase, at the onset of AlO_4 formation

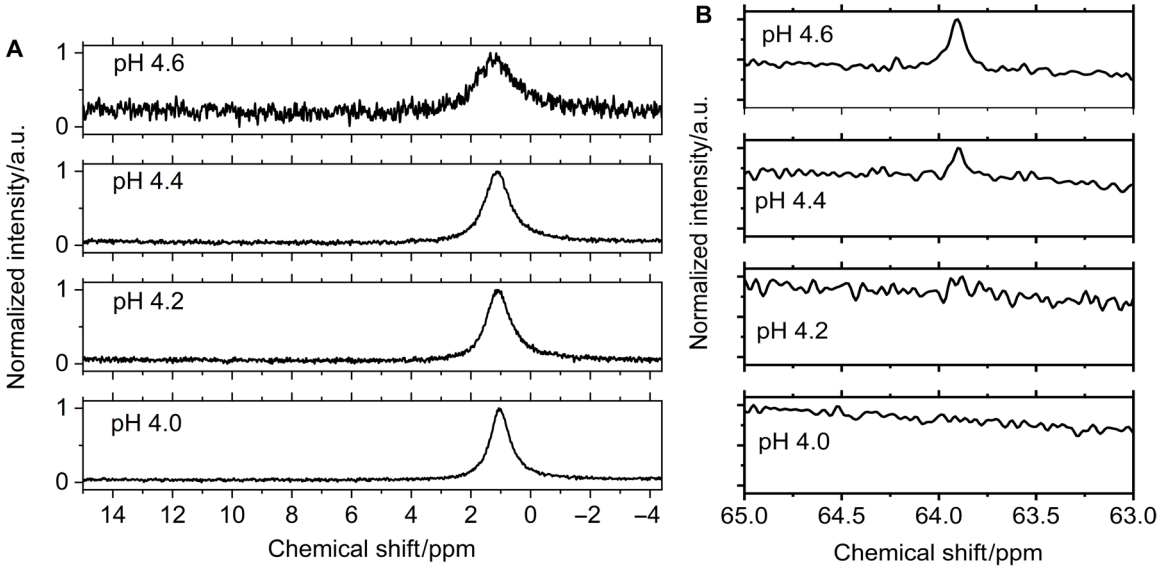

Fig. 3. Influence of pH on Al(III) speciation during the early stages of nucleation. ^{27}Al-NMR spectra at ~2.2 mM $[Al^{3+}]$ at different pH values (i.e., pH 4.0 and 4.2 in the prenucleation regime and pH 4.4 and 4.6 in the postnucleation regime): (**A**) Resonance due to monomeric species and (**B**) the spectral region of tetrahedral AlO_4 coordination (full spectra in the fig. S7). The resonance due to the tetrahedral AlO_4 environment appears only after nucleation, suggesting that corresponding irreversible chemical changes underlie phase separation. a.u., arbitrary units.

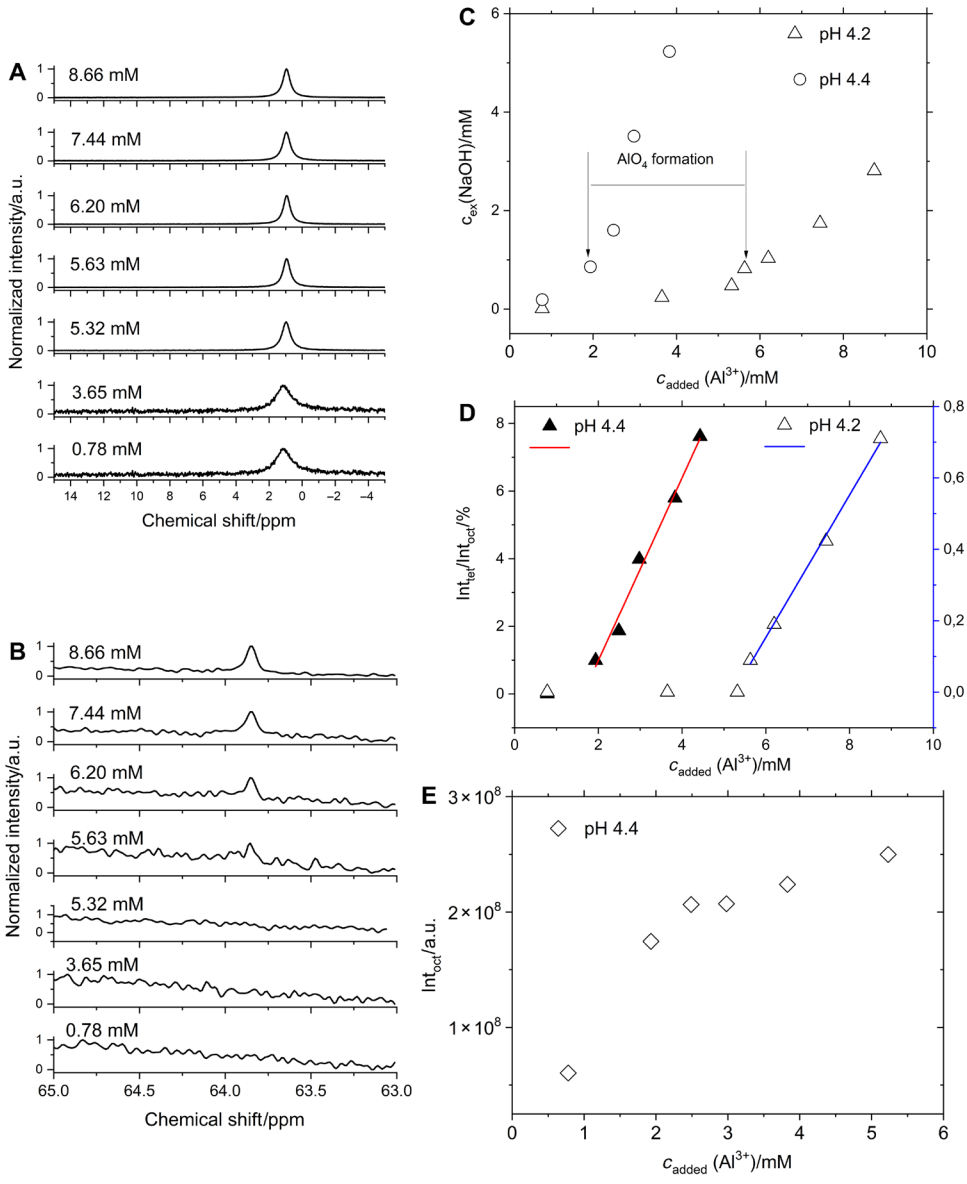

Fig. 4. Influence of concentration on Al(III) speciation during the early stages of nucleation. ^{27}Al-NMR spectra of samples drawn at specific total Al(III) concentrations as indicated in the graphs during titration experiments: (**A**) Resonance for the monomeric species and (**B**) for the AlO_4 environment at different Al(III) concentrations at pH 4.2. In combination with the titration curves (Fig. 1A) and stop experiments (Fig. 1B), this shows that tetrahedral environments emerge after nucleation. (**C**) Sampling points at pH 4.2 and 4.4 with indicated concentration of AlO_4 from NMR, confirming its appearance after the change in hydrolysis regime, i.e., after phase separation. (**D**) Evolution of the amount of tetrahedral AlO_4 species given as a percentage of the octahedral population (Int_{tet}/Int_{oct}) assessed from the intensity of integrated NMR peaks, showing a linear increase with Al(III) addition at both pH values. (**E**) Resonance intensity due to octahedral Al(III) versus the total [Al^{3+}] concentration. The amount continues to increase after AlO_4 formation at 1.93 mM [Al^{3+}] but with an altered slope, implying the existence of an intermediate dynamic (meta)stable state between octahedral and tetrahedral species.

(Fig. 4E). This indicates that the added octahedrally coordinated Al(III) species partially transform into tetrahedral Al(III) species in the postnucleation regime. However, the intensity due to the octahedrally coordinated Al(III) species still continues to increase with Al(III) addition after the formation of AlO_4 environments, implying the existence of an intermediate dynamic state between octahedral and tetrahedral species, i.e., olation PNCs. This may also help in rationalizing previous experimental observations of the conversion of dimers (that disappear fast) into tridecamers (that appear slowly) by dilution, which occurs via (these previously unidentified) intermediate species as reviewed by Akitt (*13*).

DISCUSSION

From the pH-constant titration, the release of H^+ species due to Al(III) hydrolysis can be quantitatively analyzed on the basis of the experimentally determined dependence between $[H^+]_{released}/[Al^{3+}]_{added}$. The released amount of protons, $[H^+]_{released}$, is equal to $[OH^-]_{extra}$, which is the amount of base added to keep the pH constant minus that required for adjusting the pH of the added aluminum solution. Here, the ratio $[H^+]_{released}/[Al^{3+}]_{added}$ is denoted as the parameter x, which can be plotted against the added concentration of Al(III), $[Al^{3+}]_{added}$ (see fig. S9). The values of parameter x in the prenucleation regime increase from 0.1 to 0.25, depending on the pH value.

A notable increase in the *x* parameter occurs only after nucleation, starting at Al(III) concentrations where the hydrolysis regime changes at each pH, i.e., at the onset of the formation of tetrahedral AlO_4, as evidenced by NMR measurements (see above). The development of *x* versus $[Al^{3+}]_{added}$ then asymptotically approaches a value of ~2 after nucleation. It should be pointed out that, as previously suggested, the number of released protons associated with the transformation of planar Al_{13} (octahedral) to three-dimensional Keggin-Al_{13} (with one central tetrahedral AlO_4) upon aging is two (*10*), which agrees with the asymptotical value of the parameter *x*: The development of *x* versus $[Al]_{added}$ indicates that, in the postnucleation regime, the amount of H^+ generated per Al(III) added increases continuously, mirroring an increased average tendency for the formation of tetrahedral environments.

Considering cooperative interactions due to the proximity of hydrolysis constants of the initial Al(III) hydrolysis, Martin (*8*) suggested that the total coordination number uniformly decreased with deprotonation and that the average coordination numbers of $[AlOH]^{2+}$, $[Al(OH)_2]^+$, and $[Al(OH)_3]^o$ species were 5.5, 5.0, and 4.5, respectively, depending on the respective number of water ligands. The formation of the penta-coordinated $[Al(H_2O)_4(OH)]^{2+}$ complex (*9*) and of recently theoretically predicted stable penta-coordinated $[Al(H_2O)_2(OH)_3]^o$ and tetra-coordinated $[Al(H_2O)(OH)_3]^o$ complexes in solution (*15*) supports the notion that dynamic exchanges between different coordination environments are important for the onset of phase separation. The coexistence of tetra- and penta-coordinated Al(III) species was also found on the surface of the growing gibbsite, where the transition between different coordination environments plays an important role in the crystallization process (*27*). On the other hand, since no dimeric Al(III) species were detected (*8*), Brown *et al.* (*12*) suggested that the coordination number of Al(III) decreased because of polymerization reactions. Scheck *et al.* (*28*) analyzed the entropic contribution to hydrolysis in the Fe(III) system and showed that dynamic olation reactions, that is, monohydroxo oligomerization reactions, accompany PNC formation already upon initial hydrolysis. Considering the global results of the present work, i.e., the domination of Al(III) monohydroxo species in the prenucleation stage, the existence of an equilibrium prenucleation state, the observation of nanosized, well-separated entities in the prenucleation stage, the formation of tetrahedral AlO_4 at the point of phase separation with the corresponding development of a network of aggregated particles, and the continual increase of the $[H^+]_{released}/[Al^{3+}]_{added}$ ratio with ongoing Al(III) addition in the postnucleation regime, in combination with literature results as indicated above, it is possible to propose a plausible PNC hydrolysis, condensation, and nucleation pathway of Al(III) at low driving force for phase separation.

Initially, (i) deprotonation of $[Al(H_2O)_6]^{3+}$ yields the hydrolysis product $[Al(H_2O)_5(OH)]^{2+}$, as confirmed by the determination of the corresponding equilibrium constant, consistent with the literature. On the basis of literature data (*9*), we furthermore assume that monohydroxo hydrolytic species partly undergo loss of water ligands, forming penta-coordinated $[Al(H_2O)_4(OH)]^{2+}$ species. We stress that our data provide no unambiguous scientific evidence for the existence of these penta-coordinated species, the detection of which in NMR may be hampered because of relaxation effects (see above), but they certainly serve as plausible intermediates toward the later formation of tetrahedral environments. The hexa- and penta-coordinated Al(III) species (ii) form highly dynamic olation PNCs (Fig. 5A). Fast chemical exchanges of aqua ligands on PNCs (upon increasing the total Al(III) concentration and approaching the solubility limit of $Al(OH)_3$) may eventually allow the formation of transitory tetrahedrally coordinated sites within the olation PNCs (Fig. 5B). Afterward, these tetrahedral hydroxo groups (iii) within PNCs may provide the specific geometric environment to facilitate the instantaneous deprotonation of one tetrahedral hydroxo bridge and protonation of a PNC-neighboring hydoxo ligand toward the release of a water molecule, yielding the first oxolation species (O-bridging). This induces shortening of Al—O bonds of both Al—OH and Al—OH_2 species, as well as an increase of the Al—O—H bond angles (*29*), in turn decreasing the dynamics at the tetrahedral site and rendering the formation of tetrahedrally coordinated AlO_4 species essentially irreversible (Fig. 5C). In other words, olation PNCs serve as highly dynamic solution precursors toward the formation of AlO_4 environments at specific pH values and total Al(III) concentrations at low driving force for phase separation. In this sense, the formation of tetrahedral olation sites in PNCs is the prerequisite of phase separation, which is subsequently caused by the formation of oxo bridges in these tetrahedral environments within the clusters. The as-formed clusters with less dynamic oxo bridges are then regarded phase-separated entities. In these postnucleation species, Al(III) in tetrahedral AlO_4 environments shows prolonged stability, and the phase-separated entities aggregate to form solid

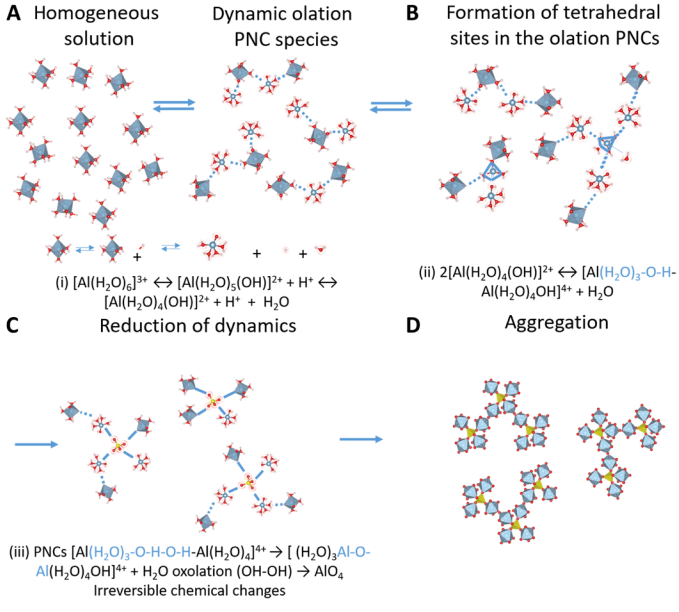

Fig. 5. Proposed mechanism for the early stages of phase separation in the aqueous Al(III) system. (**A**) Homogeneous solution of Al(III) (represented by Al octahedrons (where pale blue, red, and white colors represent Al, O, and H atoms, respectively) undergoes deprotonation reactions, yielding dynamic olation PNC species, including hexa- and penta-coordinated Al(III) environments [penta-coordinated species are represented as a ball-and-stick model with dot surface, while blue dotted lines represent olation (-OH-) bridging]. (**B**) The formation of tetrahedral (pale blue triangles) sites in the olation PNCs gives rise to an irreversible oxolation reaction. (**C**) The onset of phase separation in the Al(III) system is due to the formation of stronger bonds in AlO_4 tetrahedral environments [solid blue lines represent oxolation (-O-) bridging, while Al atoms in tetrahedral coordination after the oxolation reaction are shown in yellow]. (**D**) As-formed AlO_4 tetrahedrally coordinated species (yellow tetrahedra) get involved into further aggregation (H atoms are not shown for clarity).

material (Fig. 5D), decreasing the interfacial energy because of the demixing event and nanosolid formation (*30*). Aggregative processes in the postnucleation phase were experimentally confirmed by the TEM, Fig. 2 (C and D), and scanning electron microscopy (SEM)/energy-dispersive x-ray (EDX) analysis (fig. S9).

While Dong *et al.* (*15*) assumed that tetrahedral $[Al(H_2O)(OH)_3]^o$ species in amorphous sols can be considered as precursors of Keggin-Al_{13}, requiring the existence of small oligomeric species, our experiments show that, at low driving force for phase separation, the tetrahedral AlO_4 unit, which exists in Keggin-Al_{13} species, emerges from precursor solute PNCs species at pH values lower than that required for $Al(OH)_4^-$ formation, i.e., without the necessity of $[Al(OH)_4]^-$ preformation, aging treatment, or interaction with a specific counter anion. At the onset of phase separation, i.e., the formation of tetrahedral Al environments, PNCs also contain Al(III) species in hexa- and penta-coordinated environments, which allows rationalizing the existence of AlO_4, AlO_5, or AlO_6 coordination environments in solid samples within the PNC framework, as they are the remnants of highly dynamic species "solidified" upon phase separation of specific dynamic states under kinetic control. In this study, phase separation was not induced by forced hydrolysis conditions (e.g., base addition) but rather occurred at low driving force for phase separation, where the diffusion of Al(III) ions is the limiting process, which is also a realistic scenario in natural processes where precipitation of Al(III) plays a role. The PNC pathway of Al(III) (oxy)(hydr)oxide formation introduced in the present work may globally explain experimental results for the Al(III) hydrolysis-condensation-nucleation cascade. The fundamental process underlying the onset of phase separation in the aqueous Al(III) system is the reduction of dynamics of olation PNCs, triggered by chemical changes from olation to oxolation upon formation of tetrahedral sites in PNCs as a prerequisite.

Previously, interpretations of experimental observations in the context of Al(III) nucleation essentially relied on CNT. According to CNT, pre-/critical nuclei are thermodynamically un-/metastable and ultimately rare species (*31*). Thus, from the viewpoint of CNT, supersaturation and/or interfacial tension are the only key parameters for controlling the very early stages of precipitation. From the point of view of the PNC pathway, in contrast, the multistep reaction channel proceeding through thermodynamically stable solute precursors offers various points of attack, for instance, of organic additives, to influence the process as whole (*32*). Specifically, in the case of the aqueous Al(III) system, knowing the nature of the chemical changes that trigger the onset of phase separation, i.e., the transition from olation to oxolation within the PNCs and the role of distinct coordination environments, may thereby allow developing strategies toward stabilization/destabilization of specific chemical forms, helping to control the onset of nucleation, and/or directing the process into specific directions and, with it, synthesis outcomes. For instance, this could be achieved by providing certain geometric binding environments for PNCs on organic additives. This improved understanding seems to be an important step toward facilitating target-oriented materials synthesis (*30*), and future work should be designed toward a quantitative understanding of these processes and interactions that might eventually allow achieving the holy grail of reliable predictions of nucleation rates and tailored crystallization outcomes. Because of the broad relevance of the aqueous Al(III) system, this could potentially be exploited in various applications—from the improvement of the immobilization of heavy metal ions in environmental contexts to the development of efficient and nontoxic vaccine adjuvants.

MATERIALS AND METHODS

Potentiometric titrations at constant pH

Aluminum stock solution (0.1 M) was prepared by dissolving commercial $AlCl_3{\cdot}6H_2O$ (99%, Sigma-Aldrich) in 0.1 M HCl (0.1 M HCl standard solution, Merck). The solution was dosed into a glass beaker with a volume of 100 ml at the slowest possible dosing rate of 10 μl/min. The pH value was kept constant by counter titration with 0.05 M NaOH solution (Merck, 0.1 M NaOH standard solution). NaOH solutions were freshly prepared every day before titration experiments by dilution with fresh Milli-Q water. Aluminum hydrolysis was investigated in a specially designed system for potentiometric titrations (Metrohm, Switzerland) controlled by a central unit (905 Titrando), while the solutions were dosed by two dosing units (800 Dosino) with an internal volume of 2.0 ml each. The dosing unit for NaOH was connected with a NaOH platelets-filled column attached at the vent position of the dosing unit to prevent uptake of CO_2 from the atmosphere. The pH values were continuously monitored using a pH double-junction electrode (Metrohm) with a typical experimental error of 0.1 pH units. The calibration of the pH electrode was performed once per measurement day at three pH points (4.01, 700, and 9.21, standard solutions, Mettler Toledo) to check for any deviation in slope and intercept that can originate from interaction between Al ions with the glass membrane of the double-junction pH electrode. If the slope deviation was more than 4% from theoretical values, then the electrode was treated in 0.1 M HCl under stirring to regain the initial electrode performance. The Al(III) solution was dosed in 25 ± 0.5 ml of HCl at a specific pH value, which was finely adjusted by addition of minute amounts of 0.05 M NaOH or 0.01 M HCl before titrations. The Al(III) hydrolysis was investigated in an experimental pH range from 3.9 to 4.6. The dosing rate was 10 μl/min to provide homogeneous mixing with low driving force for phase separation, and the experimental volume was effectively stirred at the highest rate that did not yet induce formation of bubbles in the experimental volume. All titration curves are shown as the average curves of at least three measurements. At pH 3.9, the titration curve showed only a linear behavior, while the increase of the pH value induced a change in the shape of titration curves at some point, where the curves bent upward at a certain added Al(III) concentration, depending on the specific pH value.

Transmission electron microscopy

TEM measurements of samples in prenucleation and postnucleation regimes were performed on a TEM Zeiss Libra 120 operated at 120 keV, and HR-TEM analysis was performed on a JEOL JEM-2200FS with 200 keV. The samples were taken from the titration experiments at selected experimental points and blotted on a carbon-coated TEM grid, which was placed on filter paper to avoid drying artifacts by the fast removal of the excess of sample solution to the highest possible extent. Collected images were processed by iTEM (TEM) and Gatan microscopy (HR-TEM) software. The prepared samples were left to dry overnight at room temperature before measurements.

^{27}Al-NMR spectroscopy

All one-dimensional ^{27}Al-NMR experiments were conducted on a Bruker Avance III 400 MHz spectrometer operating a Broad Band

Fluorine Observation (BBFO) probe. Samples were drawn from titration experiments at pH 4.2 and 4.4 by taking 1 ml of the sample at each concentration point and filled into 5-mm (outer diameter) NMR tubes. ^{27}Al-NMR spectra were recorded subsequently by acquiring 1024 scans. The time between sampling and the measurement was approximately 12 hours for each sample. Peaks were referenced to 10 mM $Al(NO_3)_3{\cdot}9H2O$ at pH 2 as an external standard. All experimental data were acquired at a temperature of $T = 295$ K. Deuterium oxide was used for locking at a volume fraction of 5% of the total sample. TopSpin software was used for processing of raw data, while data fitting was achieved in ORIGIN software with a Levenberg-Marquardt algorithm.

Scanning electron microscopy

The sample for SEM/EDX (JSM 6610-1, JEOL, Japan) characterization has been drawn from titration experiment at pH 4.3 at 10 ks ($\approx$ 4.5 mM [Al^{3+}]) in the postnucleation regime and vacuum-filtrated through the 200-nm filter. The isolated sample was left to dry overnight at room temperature. The sample was Au-sputtered for 60 s, at 30 mA, and measured with secondary electrons at 20 kV. Because of the nature of the sample and small size of aggregates, only a few larger features were observable for SEM characterization.

SUPPLEMENTARY MATERIALS

Supplementary material for this article is available at http://advances.sciencemag.org/cgi/content/full/6/23/eaba6878/DC1

REFERENCES AND NOTES

1. G. Furrer, B. L. Phillips, K.-U. Ulrich, R. Pöthig, W. H. Casey, The origin of aluminum flocs in polluted streams. *Science* **297**, 2245–2247 (2002).
2. B. Lothenbach, G. Furrer, R. Schulin, Immobilization of Heavy Metals by Polynuclear Aluminium and Montmorillonite Compounds. *Environ. Sci. Technol.* **31**, 1452–1462 (1997).
3. C. Exley, The coordination chemistry of aluminium in neurodegenerative disease. *Coord. Chem. Rev.* **256**, 2142–2146 (2012).
4. R. Bilyy, S. Paryzhak, K. Turcheniuk, T. Dumych, A. Barras, R. Boukherroub, F. Wang, G. Yushin, S. Szunerits, Aluminum oxide nanowires as safe and effective adjuvants for next-generation vaccines. *Mater. Today* **22**, 58–66 (2019).
5. Q. Zhao, M. J. Zachman, W. I. A. Sadat, J. Zheng, L. F. Kourkoutis, L. Archer, Solid electrolyte interphases for high-energy aqueous aluminum electrochemical cells. *Sci. Adv.* **4**, eaau8131 (2018).
6. D. Lenzen, J. Zhao, S.-J. Ernst, M. Wahiduzzaman, A. Ken Inge, D. Fröhlich, H. Xu, H.-J. Bart, C. Janiak, S. Henninger, G. Maurin, X. Zou, N. Stock, A metal–organic framework for efficient water-based ultra-low-temperature-driven cooling. *Nat. Commun.* **10**, 3025 (2019).
7. H. Robatjazi, D. Weinberg, D. F. Swearer, C. Jacobson, M. Zhang, S. Tian, L. Zhou, P. Nordlander, N. J. Halas, Metal-organic frameworks tailor the properties of aluminum nanocrystals. *Sci. Adv.* **5**, eaav5340 (2019).
8. R. B. Martin, Fe^{3+} and Al^{3+} hydrolysis equilibria. Cooperativity in Al^{3+} hydrolysis reactions. *J. Inorg. Biochem.* **44**, 141–147 (1991).
9. T. W. Swaddle, J. Rosenqvist, P. Yu, E. Bylaska, B. L. Phillips, W. H. Casey, Kinetic Evidence for Five-Coordination in $AlOH(aq)^{2+}$ Ion. *Science* **308**, 1450–1453 (2005).
10. S. Bi, C. Wang, Q. Cao, C. Zhang, Studies on the mechanism of hydrolysis and polymerization of aluminum salts in aqueous solution: Correlations between the "Core-links" model and "Cage-like" Keggin-Al_{13} model. *Coord. Chem. Rev.* **248**, 441–455 (2004).
11. J.-P. Jolivet, C. Chanéac, D. Chiche, S. Cassaignon, O. Durupthy, J. Hernandez, Basic concepts of the crystallization from aqueous solutions: The example of aluminum oxy(hydroxi)des and aluminosilicates. *C. R. Geosci.* **343**, 113–122 (2011).
12. P. L. Brown, R. N. Sylva, G. E. Batley, J. Ellis, The hydrolysis of metal ions. Part 8. Aluminium(III). *J. Chem. Soc. Dalton Trans.*, 1967 (1985).
13. J. W. Akitt, Multinuclear studies of aluminium compounds. *Prog. Nucl. Magn. Reson. Spectrosc.* **21**, 1–149 (1989).
14. L. A. Wills, X. Qu, I.-Y. Chang, T. J. L. Mustard, D. A. Keszler, K. A. Persson, P. H.-Y. Cheong, Group additivity-Pourbaix diagrams advocate thermodynamically stable nanoscale clusters in aqueous environments. *Nat. Commun.* **8**, 15852 (2017).
15. S. Dong, W. Shi, J. Zhang, S. Bi, ^{27}Al NMR chemical shifts and relative stabilities of aqueous monomeric Al^{3+} hydrolytic species with different coordination structures. *ACS Earth Space Chem.* **3**, 1353–1361 (2019).
16. J. Li, C. A. Prestidge, J. Addai-Mensah, The influence of alkali metal ions on homogeneous nucleation of $Al(OH)_3$ crystals from supersaturated caustic aluminate solutions. *J. Colloid Interface Sci.* **224**, 317–324 (2000).
17. M. K. Bera, M. R. Antonio, Crystallization of keggin heteropolyanions via a two-step process in aqueous solutions. *J. Am. Chem. Soc.* **138**, 7282–7288 (2016).
18. D. Gebauer, A. Völkel, H. Cölfen, Stable prenucleation calcium carbonate clusters. *Science.* **322**, 1819–1822 (2008).
19. J. Scheck, B. Wu, M. Drechsler, R. Rosenberg, A. E. S. Van Driessche, T. M. Stawski, D. Gebauer, The molecular mechanism of iron(III) oxide nucleation. *J. Phys. Chem. Lett.* **7**, 3123–3130 (2016).
20. D. Gebauer, M. Kellermeier, J. D. Gale, L. Bergström, H. Cölfen, Pre-nucleation clusters as solute precursors in crystallisation. *Chem. Soc. Rev.* **43**, 2348–2371 (2014).
21. D. Reusser, W. H. Casey, A. Navrotsky, Energetic Insight into the Formation of Solids from Aluminum Polyoxocations. *Angew. Chem. Int. Ed.* **54**, 9253–9256 (2015).
22. D. A. Palmer, D. J. Wesolowski, Aluminum speciation and equilibria in aqueous solution: III. Potentiometric determination of the first hydrolysis constant of aluminum(III) in sodium chloride solutions to 125°C. *Geochim. Cosmochim. Acta* **57**, 2929–2938 (1993).
23. D. T. Y. Chen, Solubility products of aluminum hydroxide in various ionic solutions. *Can. J. Chem.* **51**, 3528–3533 (1973).
24. L. Allouche, C. Gérardin, T. Loiseau, G. Férey, F. Taulelle, Al_{30}: A Giant aluminum polycation. *Angew. Chem. Int. Ed.* **39**, 511–514 (2000).
25. B. C. Faust, W. B. Labiosa, K. H. Dai, J. S. MacFall, B. A. Browne, A. A. Ribeiro, D. D. Richter, Speciation of aqueous mononuclear Al(III)-hydroxo and other Al(III) complexes at concentrations of geochemical relevance by aluminum-27 nuclear magnetic resonance spectroscopy. *Geochim. Cosmochim. Acta* **59**, 2651–2661 (1995).
26. L.-O. Öhman, Comment on "speciation of aqueous mononuclear Al(III)-hydroxo and other Al(III) complexes at concentrations of geochemical relevance by aluminum-27 nuclear magnetic resonance spectroscopy" by B. C. Faust, W. B. Labiosa, K. H. Dai, J. S. MacFall, B. A. Browne, A. A. Ribeiro, and D. D. Richter. *Geochim. Cosmochim. Acta* **61**, 3257–3259 (1997).
27. J. Z. Hu, X. Zhang, N. R. Jaegers, C. Wan, T. R. Graham, M. Hu, C. I. Pearce, A. R. Felmy, S. B. Clark, K. M. Rosso, Transitions in Al Coordination during Gibbsite Crystallization Using High-Field ^{27}Al and ^{23}Na MAS NMR Spectroscopy. *J. Phys. Chem. C* **121**, 27555–27562 (2017).
28. J. Scheck, L. M. Fuhrer, B. Wu, M. Drechsler, D. Gebauer, Nucleation of hematite: A nonclassical mechanism. *Chem. Eur. J.* **25**, 13002–13007 (2019).
29. J. M. Ruiz, M. H. McAdon, J. M. Garcés, Aluminum Complexes as Models for Broensted Acid Sites in Zeolites: Structure and Energetics of $[Al(OH)_4]$-, $[Al(H_2O)_6]^{3+}$, and Intermediate Monomeric Species $[Al(OH)_x(H_2O)_{n-x}{\cdot}mH_2O]^{3-x}$ Obtained by Hydrolysis. *J. Phys. Chem. B* **101**, 1733–1744 (1997).
30. D. Gebauer, S. E. Wolf, Designing solid materials from their solute state: A shift in paradigms toward a holistic approach in functional materials chemistry. *J. Am. Chem. Soc.* **141**, 4490–4504 (2019).
31. D. Gebauer, P. Raiteri, J. D. Gale, H. Cölfen, On classical and non-classical views on nucleation. *Am. J. Sci.* **318**, 969–988 (2018).
32. D. Gebauer, How can additives control the early stages of mineralisation? *Minerals.* **8**, 179 (2018).

Acknowledgments: We thank M. Gindele for technical help during SEM measurements. **Funding:** M.J.L. acknowledges a DAAD scholarship for a postdoctoral research stay at the University of Konstanz and Leibniz University Hannover. **Author contributions:** M.J.L. and D.G. conceived the paper idea. M.J.L. performed titration experiments, partial TEM investigations, SEM/EDX measurements, sample preparations, and analyses of the results and wrote the paper. E.W. performed ^{27}Al-NMR experiments and quantitatively analyzed NMR spectra. H.R. performed HR-TEM measurements. All authors discussed the results and participated in writing. D.G. supervised the research work and wrote the paper. **Competing interests:** The authors declare that they have no competing interests. **Data and materials availability:** All data needed to evaluate the conclusions in the paper are present in the paper and/or the Supplementary Materials. Additional data related to this paper may be requested from the authors.

Submitted 23 December 2019
Accepted 8 April 2020
Published 3 June 2020
10.1126/sciadv.aba6878

Citation: M. J. Lukić, E. Wiedenbeck, H. Reiner, D. Gebauer, Chemical trigger toward phase separation in the aqueous Al(III) system revealed. *Sci. Adv.* **6**, eaba6878 (2020).

Chemical trigger toward phase separation in the aqueous Al(III) system revealed

Miodrag J. Lukic, Eduard Wiedenbeck, Holger Reiner and Denis Gebauer

Sci Adv **6** (23), eaba6878.
DOI: 10.1126/sciadv.aba6878